

Jefferson Lab at 12 GeV: The Science Program

Volker D. Burkert

Thomas Jefferson National Accelerator Facility, Newport News, Virginia 23606, USA;
email: burkert@jlab.org

Annu. Rev. Nucl. Part. Sci. 2018. 68:405–28

First published as a Review in Advance on
August 1, 2018

The *Annual Review of Nuclear and Particle Science*
is online at nucl.annualreviews.org

<https://doi.org/10.1146/annurev-nucl-101917-021129>

Copyright © 2018 by Annual Reviews.
All rights reserved

ANNUAL
REVIEWS **CONNECT**

www.annualreviews.org

- Download figures
- Navigate cited references
- Keyword search
- Explore related articles
- Share via email or social media

Keywords

nucleon spin structure, generalized parton distributions, transverse momentum distributions, 3D imaging, hadron spectroscopy, form factors

Abstract

Jefferson Lab's upgrade of its Continuous Electron Beam Accelerator Facility (CEBAF) has recently been completed. The project involved an upgrade of the accelerator to achieve a maximum beam energy of 12 GeV and the construction of a fourth end station, Experimental Hall D, as well as new detector equipment for two of the three existing halls (A, B, and C). A broad experimental program has been developed to map the nucleon's intrinsic quark distributions in transverse space and in longitudinal momentum through measurements of deeply exclusive and semi-inclusive processes, and to probe color confinement by studying the spectrum of hadrons with active gluon degrees of freedom in the wave function. Other programs include the forward parton distribution function at large quark momentum fraction x , the quark and gluon polarized distribution functions, measurements of electromagnetic form factors of the nucleon ground state and of nucleon resonance transitions at short distances, and the exploration of physics beyond the Standard Model in high-precision parity-violating processes and in the search for signals of dark matter. The higher beam energy is also suitable for exploration of quark hadronization properties using the nucleus as a laboratory. This review highlights major areas of hadron and nuclear science that will be the focus of the first 5 years of operation.

Contents

1. INTRODUCTION	406
2. THE ELECTRON ACCELERATOR AND EXPERIMENTAL EQUIPMENT	408
3. ONE-DIMENSIONAL DISTRIBUTION FUNCTIONS OF THE NUCLEON	409
3.1. Valence Quark Structure and Flavor Dependence at Large x	409
3.2. Spin Structure Functions and Parton Distributions	410
3.3. Global Analysis of Polarized Parton Densities	411
3.4. Moments of Spin Structure Functions	412
4. ELECTROMAGNETIC FORM FACTORS AT SHORT DISTANCES	413
4.1. Nucleon Elastic Electromagnetic Form Factors	413
4.2. Nucleon Resonance Transition Form Factors	413
5. SPATIAL IMAGING OF THE PROTON	413
6. UNRAVELING STRONG FORCES IN THE PROTON	415
7. TRANSVERSE MOMENTUM-DEPENDENT DISTRIBUTION FUNCTIONS AND QUARK MOMENTUM TOMOGRAPHY	418
8. GLUONIC EXCITATIONS	419
8.1. Hybrid Mesons	420
8.2. Hybrid Baryons	421
9. QUARKS AND HADRONS IN THE NUCLEAR MEDIUM	422
9.1. Color Transparency	422
9.2. Quark Propagation and Hadron Formation	422
10. SEARCH FOR NEW PHYSICS	423
10.1. Precision Experiments to Test the Standard Model of Particle Physics	423
10.2. Search for Evidence of Dark Matter	423
11. CONCLUSIONS	424

1. INTRODUCTION

Dramatic events occurred in the evolution of the microsecond-old Universe that had tremendous implications for the further development of the Universe to the state it is in today. As the Universe expanded and cooled sufficiently into the GeV range, a transition occurred from the phase of free (unconfined) quarks and gluons to the hadron phase with quarks and gluons confined in volumes of $\sim 1 \text{ fm}^3$. In the course of this process, elementary, nearly massless quarks acquire dynamical mass due to the coupling to the strong gluon field, and chiral symmetry is broken. This transition is not a simple first-order phase transition but rather a crossover between two phases of strongly interacting matter, and is moderated by the excitation of baryon resonances starting from the high-mass states and ending with the low-mass states.

A quantitative understanding of this transition requires more excited baryons of all flavors than have been observed to date (1) and are currently included in the Particle Data Group’s “Review of Particle Properties” (2). These three phenomena—the presence of the full complement of excited baryons, the acquisition of dynamical mass by light quarks, and the transition from unconfined quarks to confinement—are intricately related and are at the core of the problems we are trying to solve in hadron physics. Although we cannot recreate the exact conditions that existed during

this phase in the history of the Universe, we have all the tools at our disposal to search for new states and to study the individual states in relative isolation.

Accounting for the excitation spectrum of baryons and mesons, and describing the effective degrees of freedom, is among the most important and certainly the most challenging tasks in hadron physics today. It has been a focus of the N^* program at Thomas Jefferson National Accelerator Facility (Jefferson Lab, or JLab) at 6 GeV, and likely will remain so with the extension toward higher energies with the experiments GlueX and CLAS12.

The challenge of understanding the nucleon internal structure is still driving hadron physics research after more than 6 decades of experimental scrutiny. From the initial measurements of elastic electromagnetic form factors and the determination of parton distribution functions (PDFs) through inclusive deep-inelastic scattering (DIS), the experiments increased in statistical precision and systematic accuracy; moreover, just before the turn of the millennium, researchers realized that the PDFs represent only special cases of a more general and much more powerful way of characterizing the structure of the nucleon—the generalized parton distributions (GPDs) (3–5). In addition to information about the transverse spatial density, as encoded in the Dirac and Pauli elastic form factors $F_1(t)$ and $F_2(t)$, and the quark momentum density $q(x)$, as characterized by the PDFs, the GPDs reveal the correlation of the quarks' spatial distribution and longitudinal momentum density; in other words, they describe how the quark distributions change when the nucleon is probed at different wavelengths.

The concept of GPDs has led to new methods of “imaging” the nucleon in the form of genuine three-dimensional (3D) images in two-dimensional (2D) transverse space and one-dimensional (1D) momentum space, analogous to the computed tomography scans used in medical imaging. The mapping of the nucleon GPDs and a detailed understanding of the spatial quark and gluon structure of the nucleon have been widely recognized as key objectives of nuclear/hadron physics in the coming decades.

GPDs, as well as the more recently introduced transverse momentum–dependent distribution functions (TMDs), open up new avenues of research. The traditional means of studying the nucleon structure through electromagnetic elastic and transition form factors, and through flavor- and spin-dependent parton distributions, must also be employed with high precision to extract physics on the nucleon structure in the transition from the domain of quark confinement to the domain of asymptotic freedom. These avenues of research can be explored using the 12-GeV continuous-wave (cw) beam of the JLab upgrade, which will have much greater precision and greater kinematic reach than was possible before and will help uncover some of the remaining secrets of quantum chromodynamics (QCD) in its strong interaction domain. Also, the high luminosity that will become available with the upgrade will enable exploration of the regime of extreme quark momentum, where a single quark carries 80% or more of the nucleon's total momentum.

The strong force is mediated by the exchange of colored gluons. A quantitative understanding of the gluons' role in interactions at the lower energies and in the phenomenon of confinement, however, is still lacking. The latter is a fundamental property of visible matter and of the stability of the Universe. Models that describe the interaction through gluon flux tubes (6) infer that the glue plays an active role and can be excited and lead to novel states of mesons and baryons (hybrid states). These model predictions have been confirmed in QCD computations on the lattice (7, 8) for relatively heavy pion masses. The search for these hybrid mesons and baryons is another focus of the experiments at JLab.

In Section 2, I provide a brief overview of the JLab accelerator upgrade to 12 GeV and the experimental equipment that will be used to carry out the science program during the first 5 years of operation. Section 3 describes what we expect to learn from the high-statistics measurements to

access polarized and unpolarized PDFs at very large x . In Section 4, I discuss the program to extend the measurement of the elastic electromagnetic form factors to much higher momentum transfer. In Section 5, I describe the program to study the generalized GPDs and the 3D imaging of the nucleon quark structure in impact parameter space. Information from the GPD analysis is essential to obtain access to the gravitational form factors (GFFs) that encode basic information about the mechanical properties of the proton, such as the internal pressure distribution, the shear forces acting on the quarks, and the angular momentum distribution in the proton. These fundamental properties have been completely unknown until very recently; details are discussed in Section 6. In Section 7, I describe the TMDs and imaging in momentum space. Polarization degrees of freedom will be crucial for disentangling these fundamental distribution functions, which are necessary for the development of a multidimensional representation of quarks in the proton. In Sections 8–10, I discuss some of the other major programs, including gluonic excitations in mesons and baryons, quarks and hadrons in the nuclear medium, and the search for physics beyond the Standard Model (SM), which makes use of high-precision measurements with the upgraded electron accelerator. Finally, I draw some conclusions in Section 11.

This article is an overview and covers a broad future physics program, and does not go into detail on any of the topics discussed. I provide references to review articles that discuss the phenomenological underpinnings of much of the material, especially the parts related to GPDs and TMDs. Generally, I focus on experiments requiring higher energy at the expense of interesting measurements that use the lower energies that were already available before the JLab energy upgrade was completed.

2. THE ELECTRON ACCELERATOR AND EXPERIMENTAL EQUIPMENT

The JLab Continuous Electron Beam Accelerator Facility (CEBAF) incorporates two linear accelerators based on superconducting radiofrequency technology. Spin-polarized electrons are generated in the gun and preaccelerated and accelerated in the north linear accelerator (linac). They are then bent in a 180° arc and injected into the south linac. This process is repeated four-and-a-half times to reach the final energy for Hall D and up to four additional times for the desired delivery energies to Halls A, B, and C. In the recirculating arcs, electrons are transported in five independent out-of-phase tracks of different energies. For operation at 12 GeV, five accelerating cryomodules with four-times-higher gradients than were used in the 6-GeV machine were added to each of the two existing linacs to reach a maximum energy of 10.8 GeV for Halls A, B, and C. One more arc path and one more pass through the north linac were added to achieve the highest beam energy of 12 GeV. This beam energy is generated exclusively for Hall D, whereas the other three halls may receive beams at the same or different beam energies with differences in current of up to a factor of 10^5 , simultaneously.

Major new detectors and other experimental equipment have been installed in Halls B, C, and D that support a broad program of nuclear and hadronic physics. In Hall D, a large hermetic detector with a solenoid magnet at its core has been in operation since 2015. It incorporates tracking capabilities and photon detection over nearly the full 4π solid angle. This hall is dedicated to the production of mesons employing a linearly polarized photon beam. The new CLAS12 spectrometer in Hall B features large solid-angle coverage and luminosities of $L = 10^{35} \text{ cm}^{-2} \text{ s}^{-1}$ for electron scattering experiments with multiple particle final states, and Hall C includes a new superhigh-momentum spectrometer (SHMS) in addition to the existing high-momentum spectrometer (HMS). In Hall A, the new Super BigBite Spectrometer (SBS) has been added to the existing high-resolution spectrometer pair HRS², and other large installation experiments have

been proposed. Complementing the new equipment are a highly spin-polarized electron gun, high-power cryogenic targets, and several polarized targets using NH_3 , ND_3 , HD , and ^3He to support a broad range of polarization measurements. There are longer-term proposals for a high-precision measurement of polarized Møller scattering (9) to determine the weak mixing angle with high precision and for a large-acceptance spectrometer, SoLID, for high-luminosity measurements of parity violation in DIS and of polarized semi-inclusive DIS (SIDIS).

3. ONE-DIMENSIONAL DISTRIBUTION FUNCTIONS OF THE NUCLEON

In the late 1960s, high-energy electron scattering experiments at Stanford Linear Accelerator Center (SLAC) observed the scaling behavior of the experimental cross section of $ep \rightarrow e'X$ when plotted as a function of an appropriately defined scaling variable. The modern standard definition is $x = Q^2/2m\nu$, with $Q^2 = (e - e')^2$, where e and e' are the four-momenta of incoming and scattered electrons and $\nu = E - E'$ is the energy loss of the electron in the scattering. The scaling indicates that the coupling of the electron to the proton is point-like, which is understood as electron scattering off elementary quarks. Since then, the measurements have been refined, and it was found that the scaling is only approximate and that observed deviations from scaling are attributable to gluon radiation from quarks in the scattering $\gamma_v + q \rightarrow q + g$. Scaling violation is quantitatively understood within perturbative QCD (pQCD) and is described in the evolution equations of QCD (10–12), which have been used to determine the gluon distribution function in the proton.

3.1. Valence Quark Structure and Flavor Dependence at Large x

Spin-polarized and -unpolarized structure functions provide a window into the internal quark longitudinal momentum and helicity densities of nucleons. The study of these objects provides insight into the two defining features of QCD: (a) asymptotic freedom at small distances and (b) strong interaction and confinement at large distance scales. After more than 3 decades of measurements at several accelerator facilities worldwide, a truly impressive amount of data has been collected, covering several orders of magnitude in the kinematic variables x and Q^2 (e.g., 13–16). Yet, there are still important regions at large x where data are not available or have large uncertainties, and where significant improvements are possible through high-luminosity experiments at 12 GeV.

An open question concerns the behavior of the structure functions in the extreme kinematic limit $x \rightarrow 1$. In this region, effects from the virtual sea of quark–antiquark pairs are suppressed, making this region easier to model than the small- x region. This is also the region where QCD in its high-energy limit can make absolute predictions. The large- x domain is difficult to reach as cross sections are kinematically suppressed, the magnitude of the PDFs is small, and final-state interactions (partonic or hadronic) are significant. The first successful steps into the large- x domain were made at energies of 5–6 GeV (18–20). The interest triggered by these results and the opportunity to extend the program to larger x (for recent reviews, see References 21 and 22) made this program one of the cornerstones of the JLab 12-GeV upgrade.

The unpolarized deeply inelastic inclusive cross section for $e + p \rightarrow e' + X$ is described by the two structure functions $F_1^p(x)$ and $F_2^p(x)$, which relate to the interaction of the deeply virtual photon with the charge and current distribution in the proton. $F_2^p(x)$ has been charted in a wide range of x , leading to precise knowledge of the quark distribution $u(x)$. The corresponding neutron structure function, $F_2^n(x)$, has been well measured only for $x < 0.5$ because nuclear corrections, using deuterium as a target, are large and uncertain at $x > 0.5$. Corrections for Fermi motion

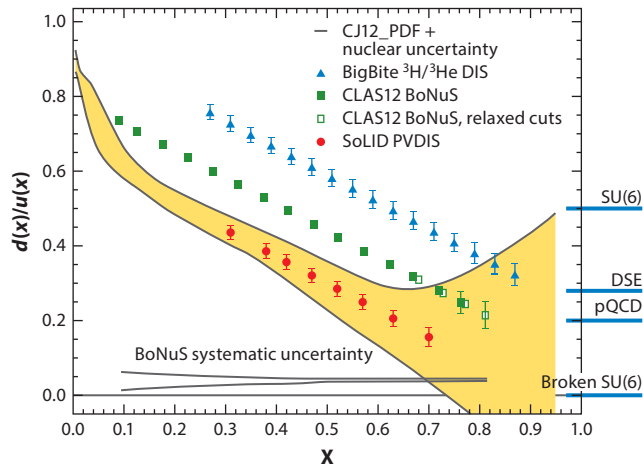


Figure 1

Projections for the ratio $d(x)/u(x)$ from the Marathon experiment (*solid triangles*), the CLAS BoNuS12 experiment (*solid squares*), and the SoLID parity-violation experiment (*red circles*). The BoNuS12 systematic errors are indicated by the solid lines at the bottom. The yellow shaded area indicates the uncertainties from previous measurements. The labels on the right indicate possible limits for $x \rightarrow 1$ projected from different models. Abbreviations: DIS, deep-inelastic scattering; DSE, Dyson–Schwinger equation; PDF, parton distribution function; PVDIS, parity-violating DIS. Adapted from the 2015 NSAC Long Range Plan.

are insufficient, as final-state interactions are significant. A new technique, tested at JLab (23), has proved very effective in reducing the nuclear binding corrections.

The experiment described in Reference 23 used a novel radial time-projection chamber with gas electron multiplier readout as a detector for the low-energy spectator proton in the reaction $en(p_s) \rightarrow ep_s X$. Measurement of the spectator proton for momenta as low as 70 MeV/c and at large angles minimizes the poorly known nuclear corrections at large x . The techniques will be used with CLAS12 to accurately determine the ratio $d(x)/u(x)$ to much larger x values with the BoNuS12 experiment (24). The Marathon experiment in Hall A (25) will measure inclusive scattering on two mirror nuclei, ^3He and ^3H , for which the nuclear wave functions are very similar. The cross-section ratio $\sigma(e^3\text{He} \rightarrow e X)/\sigma(e^3\text{H} \rightarrow e X)$ is then largely free of nuclear corrections, and the ratio of structure functions F_2^n/F_2^p and $u(x)/d(x)$ can be extracted. **Figure 1** shows the projected data for $d(x)/u(x)$ for both experiments. A dramatic improvement is projected at large x . The Marathon experiment has taken data in the spring of 2018, and the BoNuS12 experiment is scheduled to take data in 2019.

3.2. Spin Structure Functions and Parton Distributions

The lack of precise data in the domain of valence quarks and especially at very large x is quite obvious for the spin structure function $g_1(x, Q^2)$, both on the proton and, even more so, on the neutron. New experiments at 12 GeV will significantly improve our knowledge of the basic spin structure function. Two experiments will study polarized parton distributions in the range $x \leq 0.85$ on polarized protons and on polarized neutrons. Using standard detection equipment, a redesigned polarized target adapted to the CLAS12 experiment (26) can achieve high-precision results on helicity asymmetries A_1^p and A_1^n by employing longitudinally polarized NH_3 and ND_3 targets (**Figure 2**). Similar coverage is projected with the use of a polarized ^3He target in Hall

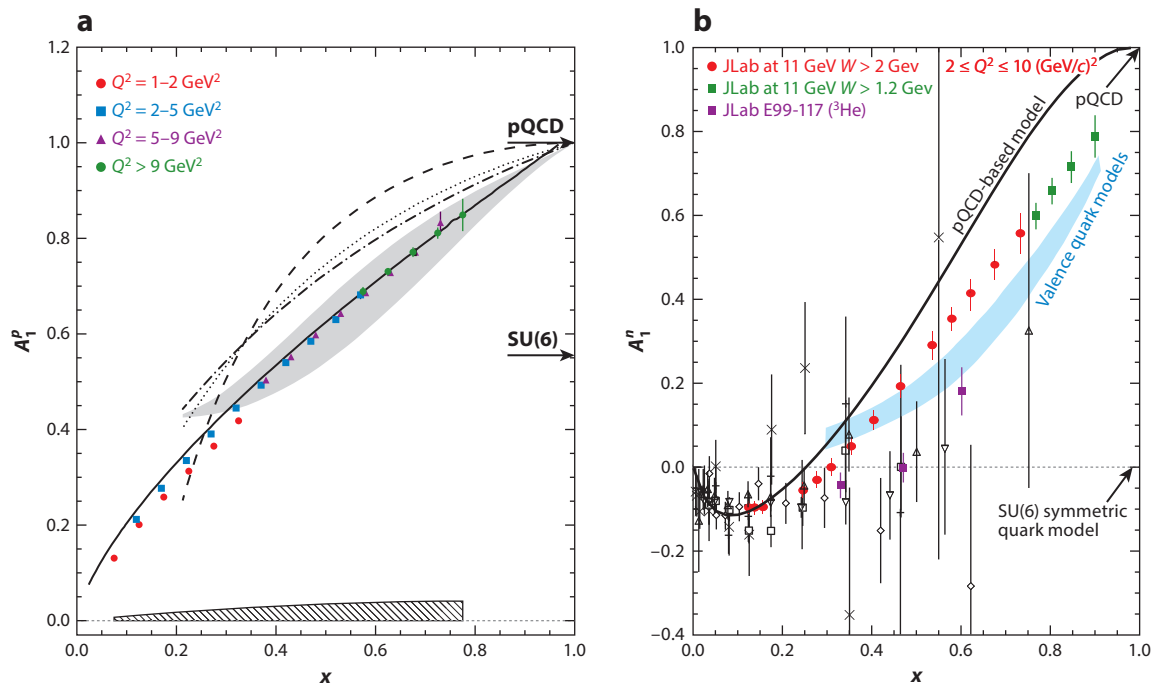


Figure 2

Projections for the double-polarization helicity asymmetries (a) A_1^p , making use of polarized NH_3 , and (b) A_1^n , using polarized ^3He . The green markers at $x > 0.8$ indicate data that include most of the nucleon resonance region, assuming the validity of the duality between the resonance and the deep-inelastic scattering regions.

$A(27)$, where most of the polarization is carried by the neutron. These data will discriminate among models in the large- x region. The projected results shown in **Figure 2** are with a $W > 2 \text{ GeV}$ constraint. Studies of hadron-parton duality will reveal whether this constraint can be relaxed so that spin structure functions may be used for $x \leq 0.9$ in the extraction of parton spin densities from global fits including these data (for a review, see Reference 16).

Results on proton and neutron targets will enable extraction of the d quark polarization, $(\Delta d + \Delta \bar{d})/(d + \bar{d})$, and the asymmetry of the polarized sea, $x[\Delta \bar{u}(x) - \Delta \bar{d}(x)]$. **Figure 3** depicts the kinematic reach and precision expected from these measurements (28).

3.3. Global Analysis of Polarized Parton Densities

The larger window that will open onto the DIS domain with the 12-GeV upgrade will enable more stringent constraints to be placed on the parton distributions in global fits to polarized structure function data. JLab data at lower energies have already had a unique impact at large x (15). The improvement resulting from the 12-GeV upgrade will also be significant at moderate x , notably for the polarized gluon distribution $\Delta G(x)$.

Significant improvements can be achieved with the expected data from experiments (26). The data will not only reduce the error band on $x\Delta G(x)$ but will also likely allow a more detailed modeling of its x dependence. Significant improvements are expected for the quark distributions as well, especially for the polarized s quark density $\Delta s(x)$.

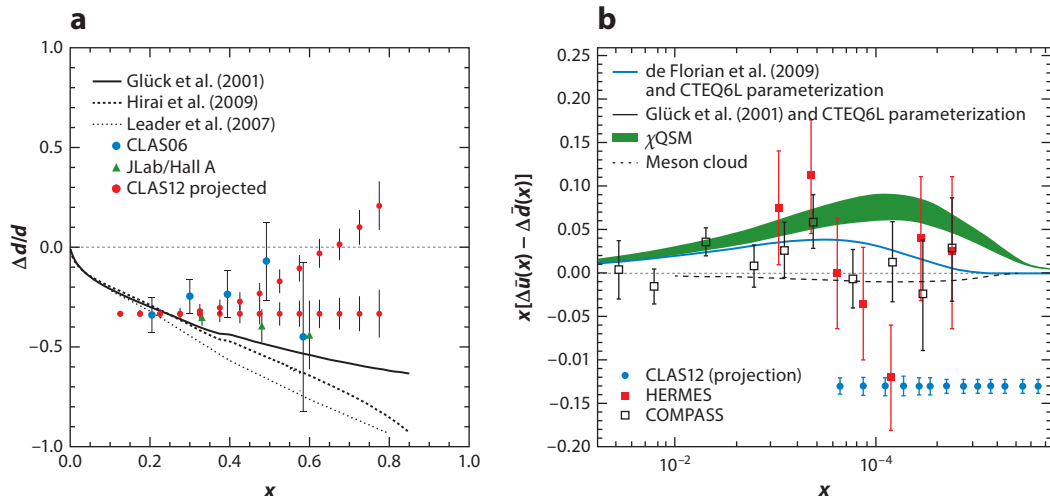


Figure 3

(a) Expected results for $(\Delta d + \Delta \bar{d})/(d + \bar{d})$ (29–31). The central values of the data follow two arbitrary curves representing two categories of predictions, namely the ones that predict $\Delta d/d$ stays negative (LO and NLO analyses of polarized DIS data) and the ones that predict $\Delta d/d \rightarrow 1$ when $x \rightarrow 1$ (LO pQCD and a quark–hadron duality scenario). (b) Projected uncertainties for the asymmetry of the polarized sea quarks (29, 32). Abbreviations: DIS, deep-inelastic scattering; LO, leading-order; NLO, next-to-leading-order; χ QSM, chiral quark soliton model.

3.4. Moments of Spin Structure Functions

Moments of structure functions are related to the nucleon’s static properties by sum rules. Inclusive DIS data obtained at JLab have permitted evaluation of the moments at low and intermediate Q^2 (17–19). With a maximum beam energy of 6 GeV, the measured fractional strength of the moments becomes rather limited for Q^2 greater than a few GeV^2 . The 12-GeV upgrade extends this range to significantly higher Q^2 values.

At sufficiently large Q^2 , the Bjorken sum rule (33) relates the integral

$$\Gamma_1^{p-n}(Q^2) = \Gamma_1^p(Q^2) - \Gamma_1^n(Q^2) = \int [g_1^p(x, Q^2) - g_1^n(x, Q^2)] dx$$

to the nucleon axial charge g_A :

$$\Gamma_1^{p-n}(Q^2 \rightarrow \infty) = \frac{1}{6} g_A.$$

The moments will be measured up to $Q^2 = 6 \text{ GeV}^2$ with a statistical accuracy improved severalfold over that of the existing world data within the measured region.

Finally, moments in the low ($\simeq 0.5\text{-GeV}^2$) to moderate ($\simeq 4\text{-GeV}^2$) Q^2 range will enable extraction of higher-twist parameters, which represent correlations between quarks in the nucleon. One can perform this extraction by studying the Q^2 evolution of the first moments (34, 35). Higher-twist contributions have consistently been found to have a smaller effect than expected. Going to lower Q^2 enhances the higher-twist effects but makes it harder to disentangle a specific high-twist contribution from even higher ones. Furthermore, the uncertainty on α_s becomes prohibitive at low Q^2 . Thus, higher twists turn out to be hard to measure. Adding data at higher Q^2 to the present JLab data set provides better separation of the individual higher twists from one another as well as from the uncertainty in α_s . The smallness of higher twists, however, requires

statistically precise measurements with small point-to-point correlated systematic uncertainties. Such precision at moderate Q^2 has not been achieved by the experiments done at high-energy accelerators, whereas JLab at 12 GeV presents the opportunity to reach such precision, considering the expected statistical and systematic uncertainties of the new experiments. The total uncertainty on the twist-4 term for the Bjorken sum f_2^{p-n} is expected to decrease by a factor of five to six in comparison to results obtained at lower energies (36).

4. ELECTROMAGNETIC FORM FACTORS AT SHORT DISTANCES

4.1. Nucleon Elastic Electromagnetic Form Factors

The most basic observables that reflect the composite nature of the nucleon are its electromagnetic form factors. The electric and magnetic form factors characterize the distributions of charge and magnetization in the nucleon as a function of spatial resolving power. These quantities can be described and related to other observables through the GPDs discussed in Section 5.

Measurements of the elastic form factors to much higher Q^2 values remain an important aspect of the physics program at 12 GeV, and will be part of the program in several experiments at JLab (37–41). The magnetic form factor of the neutron requires special experimental setups for neutron detection and the in situ neutron efficiency calibration measurement. Nucleon ground and excited states represent different eigenstates of the Hamiltonian; therefore, in order to understand the interactions underlying nucleon formation from fundamental constituents, the structure of both the ground state and the excited states must be examined.

4.2. Nucleon Resonance Transition Form Factors

The nucleon resonance transition form factors reveal the nature of the excited states and encode the transition charge and current densities on the light cone. The N^* program at JLab (for recent overviews, see References 42 and 43) has already generated results for the transition form factors at Q^2 up to 6 GeV² for the $\Delta(1232)$ and up to 7.5 GeV² for the $N(1535)3/2^+$. The latest results (44, 45) on the transition form factors of the Roper resonance $N(1440)3/2^+$, for Q^2 up to 4.5 GeV², have demonstrated the sensitivity to the degrees of freedom that are effective in the excitation of particular states (a recent review of the Roper resonance can be found in Reference 48). There are strong indications that at $Q^2 > 3$ GeV² the three-quark contributions determine the Q^2 dependence of the resonance transition amplitudes (Figure 4). The higher beam energies will extend the range to $Q^2 = 5\text{--}12$ GeV, where the transition to the coupling to elementary quarks could be fully revealed. Such measurements for several prominent excited states may serve as a benchmark to fully establish the connection to QCD approaches in the strong interaction domain. The JLab energy upgrade will enable one to probe resonance excitations at $Q^2 \leq 12$ GeV² (49), where the elementary quarks' degrees of freedom are expected to become evident in resonance formation through the approach to scaling as dressed quarks approach their elementary mass values.

Resonances in the low mass range can be measured well in single-pion production. At higher masses, resonances tend to decouple from the single-pion channel. The transition form factors of those excited states can be more effectively measured in double-pion processes such as $ep \rightarrow ep\pi^+\pi^-$ (50–52).

5. SPATIAL IMAGING OF THE PROTON

The nucleon PDFs in DIS are used to provide a 1D image of the quarks' densities $q(x)$ in longitudinal momentum (x) space. The Q^2 dependence of elastic electromagnetic form factors can be

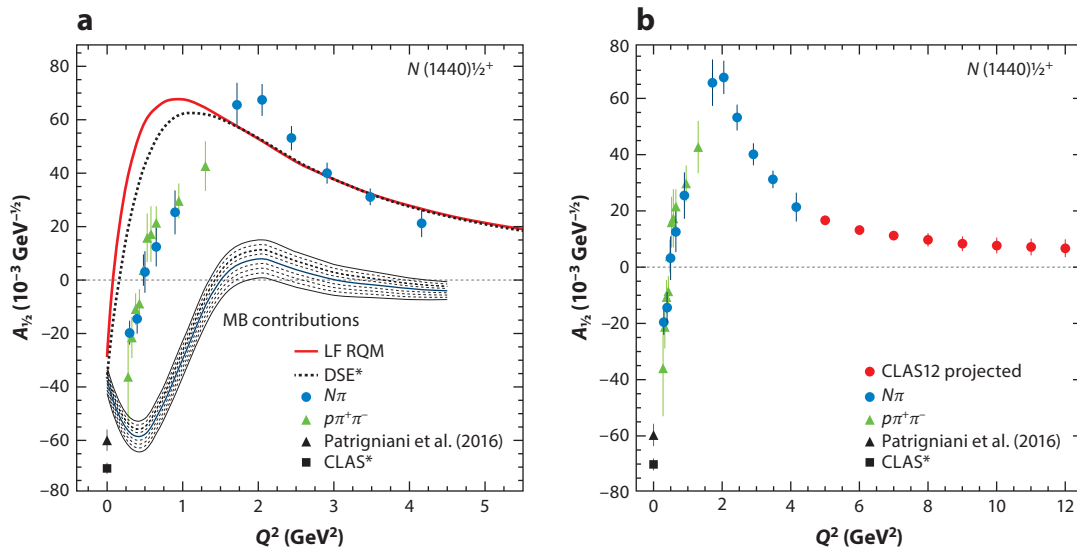


Figure 4

The Roper resonance: transverse helicity amplitude for the transition from the proton ground state to the resonant state. (a) Existing data. The solid red curve relates to the LF RQM with momentum-dependent quark masses (47). The dashed curve represents a DSE QCD (46) calculation. Both calculations describe the high- Q^2 part well. (b) Projected extension of the data to $Q^2 \approx 12 \text{ GeV}^2$. Abbreviations: DSE, Dyson–Schwinger equation; LF RQM, light-front relativistic quark model; MB, meson–baryon.

used to create a 2D projection of the charge and current densities in (transverse) impact parameter space. Both of these images are independent, and their internal correlations are lost in the projections. The GPDs allow for the construction of 3D images in correlated transverse coordinate and longitudinal momentum space. They are therefore a powerful tool for studying the internal structure of nucleons.

It is now well established (53–56) that deeply virtual Compton scattering (DVCS; the process $ep \rightarrow e'p'\gamma$) is most suitable for accessing the twist-2 vector GPDs H and E and the axial GPDs \tilde{H} and \tilde{E} in x , ξ , and t . Here, ξ is the longitudinal momentum transfer to the struck quark, and t is the four-momentum momentum transfer to the nucleon. Having access to a 3D image of the nucleon (two dimensions in transverse space, one dimension in longitudinal momentum) will give rise to completely new insights into the complex internal structure and dynamics of the nucleon that, eventually, QCD must reproduce.

The beam helicity-dependent cross-section asymmetry is defined as $A_{LU} = \Delta\sigma_{LU}/2\sigma$, where $\Delta\sigma_{LU}$ is the cross-section difference for electron spin parallel and spin antiparallel, respectively. In leading twist, $\Delta\sigma_{LU}$ is given by three GPDs (H , \tilde{H} , and E) and two form factors as

$$\Delta\sigma_{LU} \propto \sin\phi[F_1H + \xi(F_1 + F_2)\tilde{H}]d\phi,$$

where ϕ is the azimuthal angle between the electron scattering plane and the hadronic production plane. The kinematically suppressed term with GPD E is omitted. $F_1(t)$ and $F_2(t)$ are the well-known Dirac and Pauli form factors, respectively. The asymmetry is mostly sensitive to GPD $H(x, \xi, t)$. In a wide kinematics (58, 60), the beam asymmetry A_{LU} was measured at JLab at modestly high Q^2 , ξ , and t , and in a more limited kinematics (59), the cross-section difference $\Delta\sigma_{LU}$ was measured with high statistics. Moreover, the first measurements of the target asymmetry

$A_{UL} = \Delta\sigma_{UL}/2\sigma$ were carried out (61, 65, 66); here,

$$\Delta\sigma_{UL} \propto \sin\phi[F_1\tilde{H} + \xi(F_1 + F_2)H]. \quad 1.$$

The combination of A_{LU} and A_{UL} allows the separation of GPDs $H(x = \xi, \xi, t)$ and $\tilde{H}(x = \xi, \xi, t)$. By use of a transversely polarized target, one can measure the asymmetry $A_{UT} = \Delta\sigma_{UT}/2\sigma$, with

$$\sigma_{UT} \propto \cos\phi \sin(\phi - \phi_s) \frac{t}{4M^2} (F_2H - F_1E),$$

where ϕ_s is the azimuthal angle of the target polarization vector relative to the electron scattering plane. At leading order (LO), A_{UT} depends on GPD E . Measurement of A_{UT} is the most efficient and direct way to determine GPD E , as H will be well constrained by the other polarization observables, $\Delta\sigma_{LU}$ and $\Delta\sigma_{UL}$.

The first DVCS experiments carried out at JLab (57–59) and DESY (62) showed results in terms of the applicability of the handbag mechanism to probe GPDs. The handbag mechanism describes the leading contribution to the DVCS process, where the virtual photon exchanged between the electron and the proton transfers a longitudinal momentum fraction ξ to a single quark, and the same quark emits a high-energy real photon and remains in the proton. The 12-GeV upgrade offers much-improved possibilities for validating the dominance of the handbag mechanism and for accessing the GPDs.

Measurements of all three asymmetries and the unpolarized cross section will enable the separation of GPDs H , \tilde{H} , and E at some specified kinematics. To obtain a complete picture of the quark distribution in the nucleon, one needs to measure the GPDs for both u quarks and d quarks. Doing so will require measurement of DVCS not only on the proton but also on the neutron. Experiments (67) will measure the beam spin asymmetry for the neutron. If the t dependences are known, a Fourier transformation of, for instance, GPD $H^u(x = \xi, t)$ will provide information about the u quark distribution in impact parameter space, and similarly for GPDs \tilde{H}^d and E^d . **Figure 5** shows examples of simulated images of the u and d quark distributions in a transversely polarized proton using a model parameterization of GPDs (53). The detailed spatial information thus obtained can be considered analogous to X-ray imaging in computed tomography scans of live human organs.

6. UNRAVELING STRONG FORCES IN THE PROTON

Although GPDs allow for the construction of 3D images of the nucleon's internal landscape, we have little understanding of the forces intrinsic to this construction. We need to know the distribution of forces (or pressure) acting upon the quarks (and gluons) that is consistent with their binding inside the proton. Knowledge of these basic quantities of the nucleon's mechanical properties could go a long way toward obtaining a basic understanding of how QCD works in its strong interaction domain.

For a long time, this problem was considered practically unsolvable. The proton matrix element of the energy–momentum tensor (EMT) (68) contains three scalar GFFs that encode information about the angular momentum distribution $J^q(t)$ of the quarks with flavor q in transverse space, their mass–energy distribution $M_2^q(t)$, and their pressure and force distribution $d_1^q(t)$. How can we access these form factors? In analogy to probing electromagnetic properties such as charge and magnetization with photons, the mechanical properties such as mass, force, and pressure distributions on quarks can be accessed directly only in gravitational interactions. The only known process to directly measure them is elastic graviton–proton scattering, which in practice is all but impossible due to the extreme weakness of the gravitational interaction, even if an intense graviton beam could be designed and focused on a proton target.

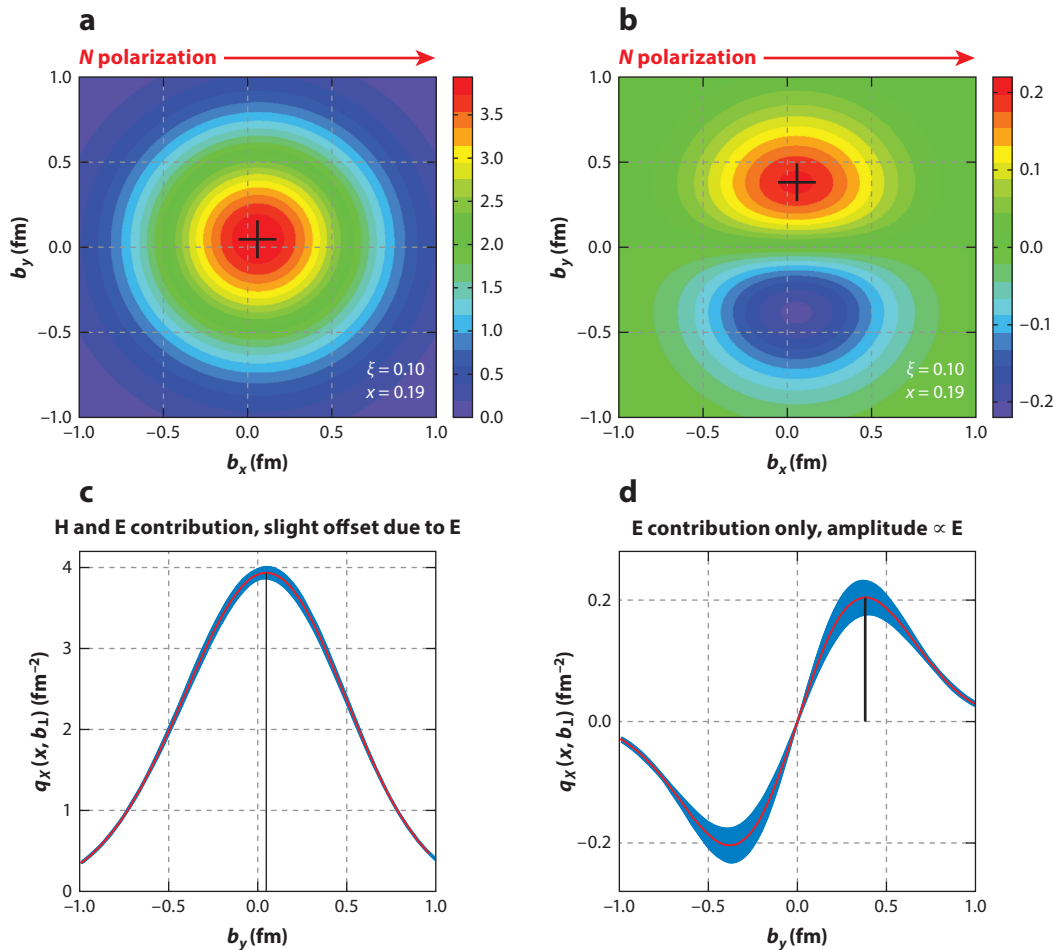


Figure 5

Tomographic images built from a t -Fourier transform of generalized parton distributions (GPDs) $E(x, t)$ and $H(x, t)$ at fixed x . (a,c) The two-dimensional image in impact parameter space (b_x, b_y) of the sum of E and H for a proton in a transversely polarized target. (b,d) The contribution of GPD E by itself, showing the splitting of negative charges (d quarks) from positive charges (u quarks). (c,d) The charge densities along b_x at $b_y = 0$. Figure adapted courtesy of F.X. Girod.

However, these same form factors also appear as moments of vector GPDs H and E (56), thus offering the potential to access the basic mechanical properties through the detailed mapping of GPDs (69). For example, the second Mellin moment of GPD $E(x, \xi, t)$ is related to the quark angular momentum distribution in the proton as

$$J^q(t) - 4/5 d_1^q(t) \xi^2 = \int_{-1}^{+1} dx x E(x, \xi, t).$$

The mass-energy and pressure distributions are related to the second Mellin moment of GPD $H(x, \xi, t)$ as

$$M_2^q(t) + 4/5 d_1^q(t) \xi^2 = \int_{-1}^{+1} dx x H(x, \xi, t).$$

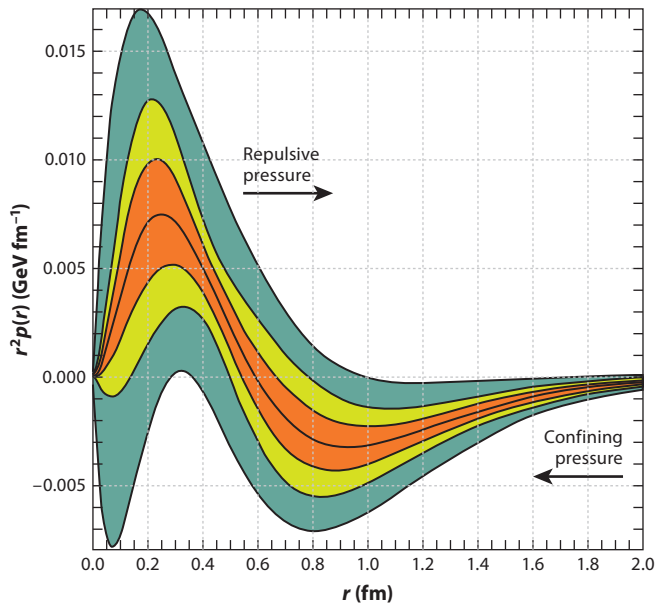


Figure 6

Radial pressure distribution in the proton determined from a measurement of Compton form factor (CFF) \mathcal{H} (70). The green shaded areas represent data from existing CLAS data and their analysis in terms of the CFFs. The inner orange shaded area represents a projection using expected results from a future experiment at higher energy and higher precision. The pressure distribution is making use of the CFF correspondence with gravitational form factor $d_1^q(t)$.

Their relative contributions are controlled by ξ .

The observables are parameterized by the Compton form factors (CFFs), which for GPD \mathcal{H} are the real quantities $\text{Re}\mathcal{H}$ and $\text{Im}\mathcal{H}$, defined by

$$\text{Re}\mathcal{H}(\xi, t) + i\text{Im}\mathcal{H}(\xi, t) = \int_{-1}^1 dx \left[\frac{1}{\xi - x - i\epsilon} - \frac{1}{\xi + x - i\epsilon} \right] H(x, \xi, t).$$

The average quark momentum fraction x is not observable in the process; it is integrated over with the quark propagators. Analytical properties of the amplitude in the LO approximation lead to the following dispersion relation:

$$\text{Re}\mathcal{H}(\xi, t) \stackrel{\text{LO}}{=} D(t) + \mathcal{P} \int_{-1}^1 dx \left(\frac{1}{\xi - x} - \frac{1}{\xi + x} \right) \text{Im}\mathcal{H}(x, t),$$

where the subtraction term $D(t)$ relates to GFF $d_1^q(t)$.

Figure 6 shows the first extraction of the pressure distribution in the proton from existing data on DVCS from CLAS (58, 60), the D -term uncertainties obtained in the global fit results from previous research (63, 64), and projected data from a planned experiment (71) to measure DVCS in a wide range of x and t and for several beam energies. These data will provide much higher precision as well as higher reach in Q^2 and momentum transfer t to the proton than has been possible before.

When experimental information on GPD $E(x, \xi, t)$ becomes available, $J^q(t)$ can be determined; through a Fourier transform, the quark angular momentum density $\rho_J(r)$ in radial space can also be determined. As discussed in Section 5, doing so requires DVCS measurement with a transversely polarized proton target.

Table 1 Leading-twist transverse momentum–dependent distribution functions

		Quark spin polarization		
		U	L	T
Nucleon polarization	U	f_1		h_1^\perp
	L		g_1	h_{1L}^\perp
	T	f_{1T}^\perp	g_T	$h_1 h_{1T}^\perp$

U, L, and T stand for transitions of unpolarized, longitudinally polarized, and transversely polarized nucleons (rows), respectively, to the corresponding quark polarizations (columns).

7. TRANSVERSE MOMENTUM-DEPENDENT DISTRIBUTION FUNCTIONS AND QUARK MOMENTUM TOMOGRAPHY

SIDIS processes, in which the leading, high-momentum hadron is detected in coincidence with the scattered lepton, were previously used for so-called flavor tagging of quarks to select contributions from different quark species. Currently, studies are focusing on SIDIS processes that encode information on the transverse momentum distributions of quarks, information that is not otherwise accessible. For example, azimuthal distributions of final-state particles in SIDIS provide access to the orbital motion of quarks and play an important role in the study of TMDs of quarks in the nucleon.

The TMDs describe transitions of a nucleon with one polarization in the initial state to a quark with another polarization in the final state. The diagonal elements of **Table 1** are the momentum, longitudinal, and transverse spin distributions of partons, and represent well-known PDFs related to the square of the leading-twist, light-cone wave functions. The off-diagonal elements are related to the overlap of wave-function amplitudes describing the different orbital angular momentum components of the nucleon. In particular, the model predictions (73) show a dominant contribution from S- and P-wave interference in the Sivers function f_{1T}^\perp , which is related to distribution of unpolarized quarks in the transversely polarized nucleon (74), as well as a significant contribution from the interference of P and D waves in the Boer–Mulders function h_1^\perp , which is related to transversely polarized quarks in unpolarized nucleons (76).

The simplest mechanism that can lead to the Boer–Mulders function h_{1T}^\perp is a correlation between the spin of the quarks and their orbital angular momentum. In combination with a final-state interaction that is, on average, attractive, a measurement of the sign of the Boer–Mulders function would reveal the correlation between the orbital angular momentum and spin of the quarks. The interplay between the parton transverse momentum and spin generating the Boer–Mulders effect (76), which appears as a $\cos 2\phi$ modulation in the azimuthal distribution of hadrons, also generates significant subleading contributions to $\cos \phi$, which have been measured in SIDIS by the EMC Collaboration and reproduced by recent measurements at CERN, HERMES, and JLab.

Direct measurements of significant transverse target spin asymmetries performed by HERMES and COMPASS (77, 78) demonstrated, for the first time, that both effects are significant. The first unambiguously measured single-spin phenomena in SIDIS, which triggered important theoretical developments, were the sizable longitudinal target and beam spin asymmetries observed at HERMES and JLab (79, 80), and recently at COMPASS. They can be interpreted in terms of higher-twist distribution functions, indicating that quark–gluon correlations are very significant (81, 82).

Recent measurements of multiplicities and double-spin asymmetries as a function of the final transverse momentum of pions in SIDIS at JLab and COMPASS (81) suggest that transverse momentum distributions may depend on the polarization of quarks and possibly on their flavor. Calculations of the transverse momentum dependence of TMDs in different models (83, 84) and on the lattice (85) indicate that the dependence of the transverse momentum distributions on the quark polarization and flavor may be very significant.

The latest measurements from polarized Drell–Yan (DY) processes at RHIC (86) and COMPASS (87) hint at a sign change between the Sivers function observed in these DY processes and the Sivers function extracted from SIDIS processes, but both the SIDIS and DY data and their comparison have to be critically analyzed and discussed. Various assumptions involved in modern extractions of TMDs from available data rely on conjectures, in particular, the transverse momentum dependence of distribution and fragmentation functions (88), making estimates of systematic errors due to those assumptions challenging (89).

A good understanding of the underlying fragmentation process in which quarks fragment into observed hadrons is crucial for accessing details of the dynamics of quarks and gluons from SIDIS. This is especially important because in fixed-target experiments one has a mixture of contributions originating from different regions: the so-called current fragmentation region, where the observed hadron is produced from the struck quark; the so-called target fragmentation region, where the hadron is produced from the remnants of the nucleon; and the intermediate fragmentation region, where the hadron is produced by the soft gluon radiation from the struck quark and nucleon remnant (90).

TMD studies will greatly benefit from the higher energy and high luminosity available at 12 GeV. A comprehensive program is in preparation at JLab to study these new quark distribution functions in great detail. Several experiments focus on measurements with high precision or covering a large phase space of charged pions and kaons on unpolarized hydrogen and deuterium targets (93–95). Experiments have also been proposed to study the SIDIS on polarized ^3He (91) and on polarized hydrogen (92). In the longer term, measurements with polarized targets have been proposed for the SoLID detector in Hall A at very high luminosity.

The experimental effort should produce high-quality asymmetry data in a wide range of the four-dimensional space (Q^2 , x , z , p_T). The combination of measurements in a wide Q^2 range from HERMES, COMPASS, and JLab would enable studies of evolution effects and control possible higher-twist contributions in the measurements of transverse spin observables, providing access to the nontrivial Q^2 evolution of the Sivers TMD. For a complete TMD program, experimental information about quark fragmentation functions will be needed from other experiments. Once this information has been assembled, the TMDs can be used to construct 3D images of the internal quark momentum distributions in longitudinal and transverse momentum space (x , k_x , k_y). A complex analysis framework and related software will be necessary in order to do so in a consistent way. **Figure 7** shows an example of simulated distributions for u and d quarks in a transversely polarized proton, employing the Sivers TMD function f_{1T}^\perp .

8. GLUONIC EXCITATIONS

The presence of gluons has been established in high-energy e^+e^- collisions, where the reaction $e^+e^- \rightarrow 3$ jets was observed. This process is predicted in pQCD and is quantitatively described as the result of hard gluon bremsstrahlung from one of the high-energy quarks in the annihilation process $e^+e^- \rightarrow q\bar{q}g$. An open question in hadron physics concerns whether gluons (i.e., the glue) actively participate in processes at low energy, such as excitations of mesons and baryons. The

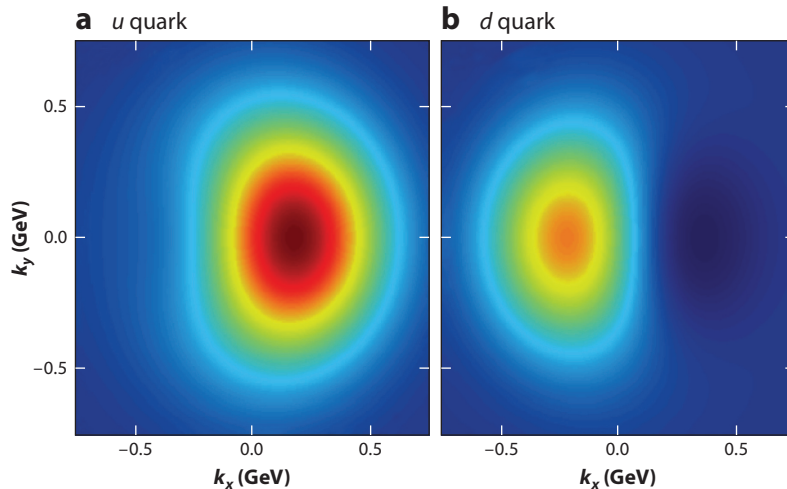


Figure 7

Simulated distributions of (a) u and (b) d quarks as a function of k_x and k_y . Each image is a two-dimensional image of unpolarized quarks in a transversely polarized proton at $x = 0.1$, shown as a tomographic slice. At 12 GeV, similar tomographic slices can be obtained for $x > 0.1$. The u quarks show an anisotropy and a shift toward positive k_x values, whereas the d quarks show the opposite anisotropy and a shift to negative k_x values. The modifications from the unpolarized case are described by the Sivers function. Figure adapted from Reference 75.

most promising way to establish the effect of the glue at low energies is through detailed study of the hadron spectrum.

8.1. Hybrid Mesons

Our understanding of how quarks form mesons has evolved within QCD, and we expect a rich spectrum of mesons that includes not only the quark (and antiquark) degrees of freedom but also gluonic degrees of freedom. Excitations of the gluon field binding the quarks (and antiquarks) can give rise to energy excitations of the glue (hybrid mesons), in addition to quark excitation levels predicted by the constituent quark model. A picture of these hybrid mesons is one in which these particles are excitations of a gluon flux tube that forms between the quark and antiquark. Such a picture may well be applicable to heavy-quark systems; whether this picture is also applicable in the light-quark sector with (constituent) quark masses ~ 350 MeV (i.e., much less than the ~ 1.2 -GeV mass of the flux tube) has been questioned (e.g., 96). Experimentally, it is particularly interesting that some of these hybrid mesons are expected to have exotic quantum numbers $J^{\text{PC}} = 0^{+-}, 1^{-+}$, and 2^{+-} that cannot be achieved in simple $q\bar{q}$ systems. In the flux tube model (97), these states do not mix with conventional meson states, dramatically simplifying the search for hybrid mesons. The possible isolation of mesons with exotic quantum numbers provides strong evidence for gluonic excitations, although it does not uniquely identify hybrid mesons. More complex configurations (e.g., $q\bar{q}q\bar{q}$ states) may have the same quantum numbers as gluonic states ($q\bar{q}G$). For this reason, it is essential to establish not only the existence of one or two states but as many states as possible so as to characterize the systematics underlying the measured spectrum. The level splitting between the ground-state flux tube and the first excited transverse modes is expected to be ~ 1.2 GeV, and lattice QCD calculations (98) indicate that the lightest exotic hybrid meson (with $J^{\text{PC}} = 1^{-+}$) has a mass of ~ 1.9 GeV.

There have been tantalizing suggestions, mainly from experiments using pion beams, that mesons with exotic quantum numbers exist. The strongest evidence is for a $\pi_1(1600)$ exotic meson with $J^{PC} = 1^{-+}$ and a mass of 1,600 MeV. Although indications have been found by several experiments, the evidence is by no means clear cut, in part due to the apparently small production rates for these states in the decay channels examined (for a recent review, see Reference 99). As of early 2018, no mesons have been uniquely identified as hybrid mesons in the exotic partial waves. The largest data sample in the so-called golden channel, $\pi^- p \rightarrow \pi^- \pi^+ \pi^- p$, has been published by the COMPASS Collaboration (100). No new meson candidates were observed in the nonexotic partial waves.

On the basis of models, we may expect the production of hybrid mesons in photon-induced reactions to be comparable to the production of ordinary mesons. Photoproduction of mesons using an ~ 9 -GeV, linearly polarized photon beam provides a unique opportunity to search for exotic hybrids. Existing data are extremely limited for charged final states, and no data exist for multiple neutral final states. To carry out such a dedicated search, the GlueX (101) program in Hall D will look at many different final states involving both charged particles and photons. Particular emphasis will be placed on those reactions that have three or more pions in the final state. The discovery potential for GlueX arises from the very high statistics, which will exceed existing photoproduction data by several orders of magnitude. The GlueX experimental search has a mass reach up to ~ 2.8 GeV to observe mesons with masses up to 2.5 GeV.

The MesonEx program (102) has pursued an alternative approach. This experiment will use a quasi-real photon beam whose energy is measured by detecting the electrons scattered from the hydrogen production target at a very forward electron scattering angle (103). The forward tagger makes use of a high-granularity, high-resolution crystal calorimeter to detect the small-angle electrons in the energy range up to 4.5 GeV. The difference from energy tagging of real photons is that quasi-real photon tagging involves only one interaction in the production target as the final-state hadrons are produced coherently in the quasi-real photoproduction process, whereas photoproduction with a real photon beam is a two-step process: The photon beam is generated by electrons undergoing bremsstrahlung in a nuclear target, which is a thin diamond or carbon radiator in the GlueX experiment, and then the photon beam interacts incoherently in the hydrogen target to produce the hadronic final state of interest.

8.2. Hybrid Baryons

So far, the search for gluonic excitations has been limited to mesons, although baryons may also be excited through gluonic degrees of freedom (104–106). Studies of hybrid baryons are just as important as those of hybrid mesons in the quest to better understand the complex confinement mechanisms in hadrons. However, gluonic baryons $qqqG$ and ordinary three-quark baryons qqq have the same quantum number—that is, they mix with ordinary baryons—making it impossible to uniquely identify them in the partial-wave analysis. One possibility is to look for an overpopulation of states with specific spin–parity J^P assignments compared with the number of such states predicted in the constituent quark model. The excited glue adds ~ 1.3 GeV to the mass of hybrid baryons, placing the lowest-mass hybrid baryons with strangeness $S = 0$ into the range 2.2–2.4 GeV.

Another possibility is to study the helicity amplitudes $A_{1/2}$ and $S_{1/2}$ and their Q^2 dependence in electroproduction processes. The different structure of hybrid baryons and ordinary three-quark baryon states should result in different Q^2 dependences for the helicity amplitudes. In particular, the $S_{1/2}$ amplitude is expected to be zero for the lowest $J^P = 1/2^+$ hybrid baryon (107), while this is not the case for three-quark systems, and $A_{1/2}$ is projected to exhibit a Q^2 dependence,

rendering it distinctly different from the corresponding three-quark baryon states. A search for hybrid baryons is planned as part of the 12-GeV program, which will employ electroproduction processes in various final states (108).

9. QUARKS AND HADRONS IN THE NUCLEAR MEDIUM

Studies of hadrons in nuclei aim to discover potential changes of their internal structure in the nuclear medium. Recent interest in the subject is largely a result of the so-called EMC effect, a measurement by the European Muon Collaboration (109) that showed significant changes in the quark distribution of heavier nuclei over deuterium. The observation has prompted numerous theoretical evaluations and model developments. While many calculations can quantitatively reproduce the measurements, a full understanding of the observation is still lacking (110). Recent efforts have focused on the study of nucleon–nucleon correlations at short distances (see Reference 111 for a review). Another direction in experimental research is the use of nuclei as a laboratory to probe phenomena that cannot be studied on free protons and neutrons, such as color coherence effects and the hadron formation process.

9.1. Color Transparency

Color transparency (CT) is a unique prediction of QCD. It implies that, under certain conditions, the nuclear medium will allow the transmission of hadrons with reduced absorption. The phenomenon of CT is predicted in the quark–gluon basis and is totally unexpected in a hadronic interaction picture. The following conditions must be present to observe CT: The interactions must create a small-sized object, namely a point-like configuration (PLC), that has a small cross section when traveling in a hadronic medium, and the distance over which it expands to its full hadronic size must be larger than the size of the nucleus. Such conditions require high enough energy transfer to the target where the virtual photon couples to PLCs, and the full hadronization occurs outside the nucleus.

CT effects have been observed at very high energies at hadron machines, but the momentum transfer at which CT sets in has not yet been determined precisely. Small increases in nuclear transparency consistent with theoretical predictions have been observed at JLab with 5–6-GeV electron beams in proton knockout from nuclei, as well as in coherent ρ^0 production on nuclei (112, 113). The energy doubling of the JLab electron accelerator to 12 GeV will provide much better conditions, which should allow observation of a significantly increased transparency with high sensitivity.

9.2. Quark Propagation and Hadron Formation

The use of electron beams at 12 GeV is suitable for addressing fundamental questions of how colored quarks struck in the interaction with high-energy photons transform into colorless hadrons. For example, how long can a colored light quark remain deconfined? The production time T_p measures this quantity. Because deconfined quarks emit gluons, T_p can be measured via medium-stimulated gluon emission, resulting in a broadening of the transverse momentum distribution of the final hadrons. Another important question is: How long does it take to form the color field of a hadron? This can be measured by the formation time T_f^b . Because hadrons interact strongly with the nuclear medium, T_f^b can be determined by measuring the attenuation of hadrons in the nuclear medium by using nuclei of different sizes.

These questions can be addressed by measuring the hadronic multiplicity ratio

$$R_M^b(z, \nu, p_T^2, Q^2, \phi) = \frac{\{[N_b^{\text{DIS}}(z, \nu, p_T^2, Q^2, \phi)]/[N_e^{\text{DIS}}(\nu, Q^2)]\}_{\big|_A}}{\{[N_b^{\text{DIS}}(z, \nu, p_T^2, Q^2, \phi)]/[N_e^{\text{DIS}}(\nu, Q^2)]\}_{\big|_D}}$$

versus all kinematical quantities. In this expression, N_b is the number of hadrons produced in DIS events, and N_e^{DIS} is the number of associated DIS electrons. The numerator corresponds to target nucleus A , and the denominator corresponds to deuterium. ν is the energy transferred by the electron, and z is the hadron energy divided by ν . In QCD-improved parton models, R_M^b is given by the ratios of sums over products of the quark distribution functions with fragmentation functions. The proposed measurement (114) will provide two to three orders of magnitude more data than any previous experiment in this energy range and will include a much larger collection of hadron species.

10. SEARCH FOR NEW PHYSICS

The SM has been highly successful in accurately accounting for a large number of experimental observations. Its predictions have been probed at the highest-energy accelerators at HERA, at the Tevatron at Fermilab, and now at the LHC at CERN. So far, no clear deviations from the SM have been identified. While most of the searches for physics beyond the SM involve very high energy accelerators where new particle types may be produced in high-energy collisions, deviations from the SM may also be observed in high-precision experiments at lower energies. At these lower energies, two types of experiments may be suitable for probing the SM: (a) very high precision experiments to search for small deviations from SM enhanced by interference effects and (b) searches for effects that are expected to occur predominantly at lower energies.

10.1. Precision Experiments to Test the Standard Model of Particle Physics

Parity-violating electron scattering may be the best tool to study possible SM-violating effects in precision measurements of the electroquark couplings that relate to the weak mixing angle $\sin^2 \theta_W$. New Physics such as quark compositeness, or the possible existence of new gauge bosons beyond the Z^0 , may cause small deviations from SM predictions at relatively low energies. Such effects may be revealed in very high precision experiments due to amplitude interferences. With the high luminosity available at JLab, such effects could be detectable. Two experiments have been proposed to measure with high precision the weak mixing angle $\sin^2 \theta_W$ in parity-violating electron–electron scattering (Møller scattering) (9) and in deep-inelastic electron scattering (115). **Figure 8** shows the SM prediction for the energy dependence of the weak mixing angle in comparison with measurements. Previous measurements indicate possible discrepancies for several of the data points, each one at the $\geq 1\sigma$ level. The red marker indicates the recent result of the Qweak experiment at JLab (118). The proposed experiment will significantly improve the precision of the experimental database.

10.2. Search for Evidence of Dark Matter

Recent satellite measurements have shown a dramatic excess of positrons ranging in energy from 10 GeV to hundreds of GeV. One of the leading interpretations for this anomaly involves the existence of a new gauge vector boson that couples weakly to e^+e^- pairs and can be produced through interaction with the dark matter in the Universe. However, the symmetries of the SM restrict the interaction of ordinary matter with such new states. Most interactions consistent with

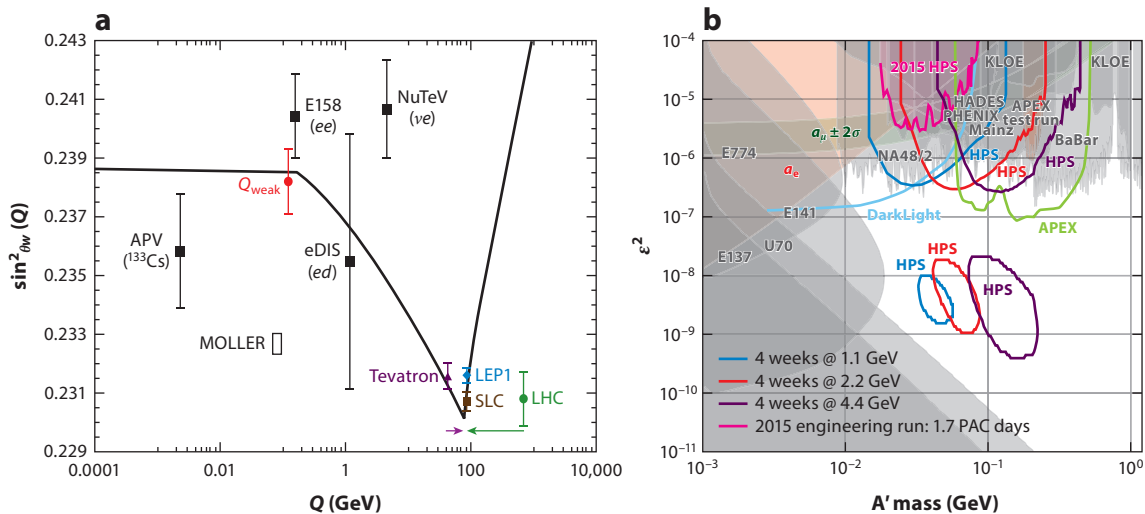


Figure 8

(a) Current knowledge of the weak mixing angle in comparison to Standard Model predictions, and the projected uncertainty from the proposed MOLLER experiment. (b) Exclusion zones for the ratio of heavy photons to electromagnetic coupling strengths to e^+e^- pairs versus the heavy-photon mass. The various lines show the exclusion zones from previous and planned measurements. The planned measurements at JLab are indicated by the lines marked HPS and APEX. The zones at top show where the HPS and APEX experiments will search for narrow peaks in the mass spectrum of the e^+e^- pair. The zone marked HPS at bottom includes the search for detached vertices that would indicate the presence of a long-lived A' with weak coupling.

SM gauge symmetries and Lorentz invariance have couplings suppressed by a large mass scale. One of the few unsuppressed interactions is the coupling of charged SM particles to a new gauge boson, A' , which is quite poorly constrained for small coupling constants.

Heavy photons mix with the ordinary photon through kinetic mixing, which induces their weak coupling to electrons: $\epsilon \approx 10^{-3}$. Because they couple to electrons, heavy photons are radiated in electron scattering and can subsequently decay into narrow e^+e^- resonances that can be observed above the copious quantum electrodynamic background. For suitably small couplings, heavy photons travel detectable distances before decaying, providing a second signature. Two experiments have been approved at JLab to considerably extend the kinematic zone covered by experiments in the search for the A' . The APEX experiment in Hall A (116) uses high-resolution magnetic spectrometers to search for narrow structures in the e^+e^- mass spectrum. The HPS experiment in Hall B (117), while also searching for bumps in the e^+e^- mass spectrum, focuses on the search for detached vertices from the decay of a long-lived A' . The experiment probes a region with much weaker coupling of the A' to e^+e^- pairs (**Figure 8b**).

11. CONCLUSIONS

The JLab energy upgrade and the new experimental equipment are well suited to an exciting scientific program aimed at performing precision studies of the complex hadron structure. The GPDs and TMDs provide fundamentally new insights into the complex multidimensional quark structure of the nucleon. Second moments of GPDs provide access to the GFFs of the EMT and, therefore, to the basic mechanical properties of the proton, such as the shear forces and the pressure distribution acting upon the elementary quarks and gluons. Knowledge of the GFFs can have a strong impact on the central question of hadron physics: how quark confinement in the proton

is realized from QCD. The exploration of the gluonic excitations of hadrons is a complementary effort to study the active role the glue plays in the meson and baryon excitation spectrum. The high precision afforded by the high luminosity, combined with the large-acceptance detectors, and the development of novel techniques to measure scattering off nearly free neutrons will enable the study of phase-space domains with extreme conditions that could not be studied before. Extremely high luminosity measurements will probe part of the phase space where deviations from the SM might be observed.

This review has selectively covered a science program that could be realized within the first 5 years of operation at the 12-GeV cw electron facility at JLab, a program that has significant discovery potential. It will provide new insights into the inner workings of strong interaction QCD and will help elucidate how the strong interaction brings about the confinement of colored quarks and gluons.

DISCLOSURE STATEMENT

The author is not aware of any affiliations, memberships, funding, or financial holdings that might be perceived as affecting the objectivity of this review.

ACKNOWLEDGMENTS

I thank Harut Avakian for contributing a major part of Section 7, and Sebastian Kuhn for useful comments and suggestions. The writing of this review was carried out under US Department of Energy contract DE-AC05-06OR23177.

LITERATURE CITED

1. Bazavov A, et al. *Phys. Rev. Lett.* 113:072001 (2014)
2. Patrignani C, et al. (Part. Data Group) *Chin. Phys. C* 40:100001 (2016)
3. Müller D, et al. *Fortschr. Phys.* 42:101 (1994)
4. Ji X. *Phys. Rev. Lett.* 78:610 (1997)
5. Radyushkin AV. *Phys. Lett. B* 380:417 (1996)
6. Isgur N, Paton JE. *Phys. Rev. D* 31:2910 (1985)
7. Dudek JJ. *Phys. Rev. D* 84:074023 (2011)
8. Dudek JJ, Edwards RG. *Phys. Rev. D* 85:054016 (2012)
9. Hafidi K, et al. (CLAS Collab.) *JLab experiment E12-06-106*. https://www.jlab.org/exp_prog/proposals/06/PR12-06-106.pdf (2006)
10. Dokshitzer YL. *Sov. Phys. JETP* 46:641 (1977)
11. Gribov VN, Lipatov LN. *Sov. J. Nucl. Phys.* 15:438 (1972)
12. Altarelli G, Parisi G. *Nucl. Phys. B* 126:298 (1977)
13. Hou TJ, et al. *Phys. Rev. D* 95:034003 (2017)
14. Alekhin S, Bluemlein J, Moch S, Placakyte R. *Phys. Rev. D* 96:014011 (2017)
15. Sato N, et al. (JLab Lab Angular Momentum Collab.) *Phys. Rev. D* 93:074005 (2016)
16. Kuhn SE, Chen J-P, Leader E. *Prog. Part. Nucl. Phys.* 63:1 (2009)
17. Fersch R, et al. (CLAS Collab.) *Phys. Rev. C* 96:065208 (2017)
18. Guler N, et al. (CLAS Collab.) *Phys. Rev. C* 92:055201 (2015)
19. Prok Y, et al. (CLAS Collab.) *Phys. Rev. C* 90:025212 (2014)
20. Amarian M, et al. (JLab E94-010 Collab.) *Phys. Rev. Lett.* 92:022301 (2004)
21. Christy ME, Melnitchouk W. *J. Phys. Conf. Ser.* 299:012004 (2011)
22. Chen JP, Deur A, Kuhn S, Meiziani ZE. *J. Phys. Conf. Ser.* 299:012005 (2011)
23. Tkachenko S, et al. (CLAS Collab.) *Phys. Rev. C* 89:045206 (2014); Addendum. *Phys. Rev. C* 90:059901 (2014)

24. Bueltman S, et al. *JLab experiment E12-06-113*. https://www.jlab.org/exp_prog/proposals/10/OPR12-6-113-pac36.pdf (2006)
25. Petratos G, et al. *JLab experiment E12-10-103*. https://www.jlab.org/exp_prog/proposals/10/PR12-10-103.pdf (2010)
26. Kuhn S, et al. *JLab experiment E12-06-109*. https://www.jlab.org/exp_prog/proposals/06/PR12-06-109.pdf (2006)
27. Zheng X, et al. *JLab experiment E12-06-110*. https://www.jlab.org/exp_prog/proposals/06/PR12-06-110.pdf (2006)
28. Hafidi K, et al. (CLAS Collab.) *JLab experiment E12-09-007*. https://www.jlab.org/exp_prog/proposals/09/PR12-09-007.pdf (2009)
29. Glück M, Reya E, Stratmann M, Vogelsang W. *Phys. Rev. D* 63:094005 (2001)
30. Hirai M, et al. (Asymmetry Anal. Collab.) *Nucl. Phys. B* 813:106 (2009)
31. Leader E, Sidorov AV, Stamenov DV. *Phys. Rev. D* 75:074027 (2007)
32. de Florian D, Sassot R, Stratmann M, Vogelsang W. *Phys. Rev. D* 80:034030 (2009)
33. Bjorken JD. *Phys. Rev.* 148:1467 (1966)
34. Osipenko M, et al. *Phys. Rev. D* 71:054007 (2005)
35. Chen JP, Deur A, Meziani Z-E. *Mod. Phys. Lett. A* 20:2745 (2005)
36. Deur A, et al. *Phys. Rev. Lett.* 93:212001 (2004)
37. Gilfoyle G, et al. *JLab experiment E12-07-194*. https://www.jlab.org/exp_prog/proposals/07/PR12-07-104.pdf (2007)
38. Wojtsekowski B, et al. *JLab experiment E12-07-109*. https://www.jlab.org/exp_prog/proposals/07/PR12-07-109.pdf (2007)
39. Wojtsekowski B, et al. *JLab experiment E12-09-019*. https://www.jlab.org/exp_prog/proposals/09/PR12-09-019.pdf (2009)
40. Wojtsekowski B, et al. *JLab experiment E12-09-016*. https://www.jlab.org/exp_prog/proposals/09/PR12-09-016.pdf (2009)
41. Wojtsekowski B, et al. *JLab experiment E12-07-018*. https://www.jlab.org/exp_prog/proposals/07/PR12-07-108.pdf (2007)
42. Aznauryan IG, Burkert VD. *Prog. Part. Nucl. Phys.* 67:1 (2012)
43. Aznauryan I, Burkert VD, Lee T-SH, Mokeev VI. *J. Phys. Conf. Ser.* 299:012008 (2011)
44. Aznauryan IG, et al. (CLAS Collab.) *Phys. Rev. C* 80:055203 (2009)
45. Aznauryan IG, et al. (CLAS Collab.) *Phys. Rev. C* 78:045209 (2008)
46. Segovia J, et al. *Phys. Rev. Lett.* 115:171801 (2015)
47. Aznauryan IG, Burkert VD. arXiv:1603.06692 [hep-ph] (2016)
48. Burkert VD, Roberts CD. arXiv:1710.02549 [nucl-ex] (2017)
49. Gothe R, et al. *JLab experiment E12-09-003*. https://www.jlab.org/exp_prog/proposals/09/PR12-09-003.pdf (2009)
50. Isupov EL, et al. (CLAS Collab.) *Phys. Rev. C* 96:025209 (2017)
51. Mokeev VI, et al. *Phys. Rev. C* 93:025206 (2016)
52. Ripani M, et al. (CLAS Collab.) *Phys. Rev. Lett.* 91:022002 (2003)
53. Burkardt M. *Int. J. Mod. Phys. A* 18:173 (2003)
54. Belitsky AV, Ji XD, Yuan F. *Phys. Rev. D* 69:074014 (2004)
55. Belitsky AV, Müller D, Kirchner A. *Nucl. Phys. B* 629:323 (2002)
56. Ji XD. *Phys. Rev. D* 55:7114 (1997)
57. Stepanyan S, et al. (CLAS Collab.) *Phys. Rev. Lett.* 87:182002 (2001)
58. Girod FX, et al. (CLAS Collab.) *Phys. Rev. Lett.* 100:162002 (2008)
59. Camacho CM, et al. (JLab Hall A Collab., Hall A DVCS Collab.) *Phys. Rev. Lett.* 97:262002 (2006)
60. Jo HS, et al. (CLAS Collab.) *Phys. Rev. Lett.* 115:212003 (2015)
61. Chen S, et al. (CLAS Collab.) *Phys. Rev. Lett.* 97:072002 (2006)
62. Airapetian A, et al. (HERMES Collab.) *Phys. Rev. Lett.* 87:182001 (2001)
63. Kumerički K, Müller D. *Nucl. Phys. B* 841:1 (2010)
64. Müller D, Lautenschlager T, Passek-Kumericki K, Schaefer A. *Nucl. Phys. B* 884:438 (2014)

65. Pisano S, et al. (CLAS Collab.) *Phys. Rev. D* 91:052014 (2015)
66. Seder E, et al. (CLAS Collab.) *Phys. Rev. Lett.* 114:032001 (2015); Addendum. *Phys. Rev. Lett.* 114:089901 (2015)
67. Fradi A, et al. (CLAS Collab.) *JLab experiment E12-11-003*. https://www.jlab.org/exp_prog/proposals/11/PR12-11-003.pdf (2011)
68. Pagels H. *Phys. Rev.* 144:1250 (1966)
69. Polyakov MV. *Phys. Lett. B* 555:57 (2003)
70. Burkert VD, Elouadrhiri L, Girod FX. *Nature* 557:396 (2018)
71. Elouadrhiri L, et al. (CLAS Collab.) *JLab experiment E12-16-010B*. https://www.jlab.org/exp_prog/proposals/16/PR12-16-010B.pdf (2016)
72. Deleted in proof
73. Pasquini B, Yuan F. *Phys. Rev. D* 81:114013 (2010)
74. Sivers DW. *Phys. Rev. D* 43:261 (1991)
75. Accardi A, et al. *Eur. Phys. J. A* 52:268 (2016)
76. Boer D, Mulders PJ. *Phys. Rev. D* 57:5780 (1998)
77. Airapetian A, et al. (HERMES Collab.) *Phys. Lett. B* 693:11 (2010)
78. Alekseev MG, et al. (COMPASS Collab.) *Phys. Lett. B* 692:240 (2010)
79. Airapetian A, et al. (HERMES Collab.) *Phys. Rev. Lett.* 84:4047 (2000)
80. Avakian H, et al. (CLAS Collab.) *Phys. Rev. D* 69:112004 (2004)
81. Avakian H, Bressan A, Contalbrigo M. *Eur. Phys. J. A* 52:150 (2016); Erratum. *Eur. Phys. J. A* 52:165 (2016)
82. Lorc C, Pasquini B, Schweitzer P. *J. High Energy Phys.* 1501:103 (2015)
83. Pasquini B, Cazzaniga S, Boffi S. *Phys. Rev. D* 78:034025 (2008)
84. Bourrely C, Buccella F, Soffer J. *Phys. Rev. D* 83:074008 (2011)
85. Musch BU, Hagler P, Negele JW, Schafer A. *Phys. Rev. D* 83:094507 (2011)
86. Adamczyk L, et al. (STAR Collab.) *Phys. Rev. Lett.* 116:132301 (2016)
87. Aghasyan M, et al. (COMPASS Collab.) *Phys. Rev. Lett.* 119:112002 (2017)
88. Anselmino M, et al. *J. High Energy Phys.* 1704:046 (2017)
89. Signori A, Bacchetta A, Radici M, Schnell G. *J. High Energy Phys.* 1311:194 (2013)
90. Boglione M, et al. *Phys. Lett. B* 766:245 (2017)
91. Wojtsekowski B, et al. *JLab experiment E12-09-018*. https://www.jlab.org/exp_prog/proposals/09/PR12-09-018.pdf (2009)
92. Avakian H, et al. *JLab experiment E12-09-009*. https://www.jlab.org/exp_prog/proposals/09/PR12-09-009.pdf (2009)
93. Avakian H, et al. *JLab experiment E12-06-112*. https://www.jlab.org/exp_prog/proposals/06/PR12-06-112.pdf (2006)
94. Contalbrigo M, et al. *JLab experiment E12-09-008*. https://www.jlab.org/exp_prog/proposals/09/PR12-09-008.pdf (2009)
95. Ent R, et al. *JLab experiment E12-09-017*. https://www.jlab.org/exp_prog/proposals/09/PR12-09-017.pdf (2009)
96. Roberts CD. *Few-Body Syst.* 58:5 (2017)
97. Barnes T, Close FE, Swanson ES. *Phys. Rev. D* 52:5242 (1995)
98. Dudek JJ, et al. *Phys. Rev. D* 83:111502 (2011)
99. Meyer CA, Swanson ES. *Prog. Part. Nucl. Phys.* 82:21 (2015)
100. Adolph C, et al. (COMPASS Collab.) *Phys. Rev. D* 95:032004 (2017)
101. Meyer C, et al. *JLab experiment E12-06-102*. https://www.jlab.org/exp_prog/proposals/06/PR12-06-102.pdf (2006)
102. Rizzo A. (CLAS Collab.) *J. Phys. Conf. Ser.* 689:012022 (2016)
103. Battaglieri M, et al. *JLab experiment E12-11-005*. https://www.jlab.org/exp_prog/proposals/11/PR12-11-005.pdf (2011)
104. Edwards RG, Dudek JJ, Richards DG, Wallace SJ. *Phys. Rev. D* 84:074508 (2011)
105. Barnes T, Close FE. *Phys. Lett. B* 128:277 (1983)

106. Barnes T, Close FE. *Phys. Lett. B* 123:89 (1983)
107. Li ZP, Burkert V, Li ZJ. *Phys. Rev. D* 46:70 (1992)
108. d'Angelo A, et al. *JLab experiment E12-16-010*. https://www.jlab.org/exp_prog/proposals/16/PR12-16-010.pdf (2016)
109. Aubert JJ, et al. (Eur. Muon Collab.) *Phys. Lett. B* 123:275 (1983)
110. Arrington J. (JLab E03-103 Collab.) *J. Phys. Conf. Ser.* 69:012024 (2007)
111. Hen O, Miller GA, Piasetzky E, Weinstein LB. *Rev. Mod. Phys.* 89:045002 (2017)
112. Hafidi K, et al. *JLab experiment E12-06-106*. https://www.jlab.org/exp_prog/proposals/06/PR12-06-106.pdf (2006)
113. Dutta D, et al. *JLab experiment E12-06-107*. https://www.jlab.org/exp_prog/proposals/06/PR12-06-107.pdf (2006)
114. Brooks W, et al. *JLab experiment E12-06-117*. https://www.jlab.org/exp_prog/proposals/06/PR12-06-117.pdf (2006)
115. Souder P, et al. *JLab experiment E12-10-007*. https://www.jlab.org/exp_prog/proposals/10/PR12-10-007.pdf (2010)
116. Woiitsekhowski B, et al. *JLab experiment E12-09-009*. https://www.jlab.org/exp_prog/proposals/10/PR12-10-009.pdf (2010)
117. Jaros J, et al. *JLab experiment E12-11-006*. https://www.jlab.org/exp_prog/proposals/11/PR12-11-006.pdf (2011)
118. Androić D, et al. (Qweak Collab.) *Nature* 557:207 (2018)

Contents

Guido Altarelli <i>Luciano Maiani and Guido Martinelli</i>	1
Multiquark States <i>Marek Karliner, Jonathan L. Rosner, and Tomasz Skwarnicki</i>	17
Penning-Trap Mass Measurements in Atomic and Nuclear Physics <i>Jens Dilling, Klaus Blaum, Maxime Brodeur, and Sergey Eliseev</i>	45
Dispersion Theory in Electromagnetic Interactions <i>Barbara Pasquini and Marc Vanderhaeghen</i>	75
Progress in Measurements of 0.1–10 GeV Neutrino–Nucleus Scattering and Anticipated Results from Future Experiments <i>Kendall Mahn, Chris Marshall, and Callum Wilkinson</i>	105
Structure of $S = -2$ Hypernuclei and Hyperon–Hyperon Interactions <i>Emiko Hiyama and Kazuma Nakazawa</i>	131
Deep Learning and Its Application to LHC Physics <i>Dan Guest, Kyle Cranmer, and Daniel Whiteson</i>	161
The Construction of ATLAS and CMS <i>Michel Della Negra, Peter Jenni, and Tejinder S. Virdee</i>	183
Small System Collectivity in Relativistic Hadronic and Nuclear Collisions <i>James L. Nagle and William A. Zajc</i>	211
From Nuclei to the Cosmos: Tracing Heavy-Element Production with the Oldest Stars <i>Anna Frebel</i>	237
Silicon Calorimeters <i>J.-C. Brient, R. Rusack, and F. Sefkow</i>	271
Automatic Computation of One-Loop Amplitudes <i>Celine Degrande, Valentin Hirschi, and Oliver Mattelaer</i>	291
On the Properties of Neutrinos <i>A. Baba Balantekin and Boris Kayser</i>	313

Heavy Ion Collisions: The Big Picture and the Big Questions <i>Wit Busza, Krishna Rajagopal, and Wilke van der Schee</i>	339
Particle Acceleration by Supernova Shocks and Spallogenic Nucleosynthesis of Light Elements <i>Vincent Tatischeff and Stefano Gabici</i>	377
Jefferson Lab at 12 GeV: The Science Program <i>Volker D. Burkert</i>	405
Dark Matter Searches at Colliders <i>Antonio Boveia and Caterina Doglioni</i>	429

Errata

An online log of corrections to *Annual Review of Nuclear and Particle Science* articles may be found at <http://www.annualreviews.org/errata/nucl>